

Imaging a GaAlAs laser diode in operation using apertureless scanning near-field optical microscopy*

G. Wurtz, R. Bachelot^a, and P. Royer

Laboratoire de Nanotechnologie et d'Instrumentation Optique, Université de Technologie de Troyes,
12 rue Marie Curie, B.P. 2060, 10010 Troyes Cedex, France

Received: 20 July 1998 / Accepted: 13 October 1998

Abstract. We report the local study of an operating double hetero-junction GaAs/GaAlAs laser diode by apertureless Scanning Near-field Optical Microscopy (SNOM). This study allows the characterization of the spatial properties of the light emitted by the laser source. The optical probe used is a tungsten tip vibrating (at frequency f) perpendicularly to the emitting surface. Suitable experimental parameters permitting us to accede to near-field information have been defined. This has led to an experimental configuration in which the probe vibration amplitude is “optimal”. A far-field detection at grazing angle is used and a second harmonic (at frequency $2f$) lock-in detection is performed. This configuration has permitted us to obtain SNOM images in stimulated emission as well as in spontaneous emission. Above the threshold current, information concerning the emitted laser mode are obtained, whereas in spontaneous emission the SNOM images are linked to the index contrast of the laser diode front facet.

PACS. 61.16.Ch Scanning probe microscopy: scanning tunneling, atomic force, scanning optical, magnetic force, etc. – 42.30.Va Image forming and processing – 42.55.Px Semiconductor lasers; laser diodes

1 Introduction

The spatial dimensions of the active surface of the semiconductor lasers are generally roughly equal to the wavelength (λ) of the visible light used in conventional optical microscopy. Consequently, the spatial properties of the emitted light of these optically active samples cannot be studied with precision by classical optical methods. This is due to the diffraction limit given by the Rayleigh criterion.

Nevertheless, the local physical characterization of these opto-electronic components would have several interests:

- detection of the local defects in the emitting area which can result from epitaxial growth inhomogeneities;
- detection of both local carriers leakage and nonradiative defects;
- direct reading and control of the modes generated in near-field zone by the wave guide.

Some teams have recently undertaken this study [1–3] by using aperture Scanning Near-field Optical Microscopy. In this technique, a small aperture (diameter $\ll \lambda$) in a metallic screen, placed at a small distance ($\ll \lambda$) from the sample surface, picks-up the optical near-field [4,5], permitting the direct reading of the emission profile of the laser diode.

The purpose of this paper is to show that this study is also possible by using apertureless probes. Contrary to the “aperture SNOM”, the “apertureless SNOM” uses an homogeneous sharp tip. This tip, whose extremity can be viewed as an electromagnetic nanoantenna, is immersed in the optical near-field of the sample to convert it in propagating waves which are far-field detectable [6–9]. The main advantages, compared to aperture SNOM, are its high resolution capability [8], as well as a larger accessible wavelength range [9]. In addition, the use of the already existing probes for AFM (Atomic Force Microscopy), (dielectric, metallic and semi-conductive probes), and STM (Scanning Tunneling Microscopy) is possible.

Our study has laid emphasis on the determination of the experimental parameters to obtain near-field information which seem to be directly linked to the local physical properties of the studied sample. Moreover, this work should contribute to a best comprehension of the signal formation in this new type of experimental configuration (*i.e.* apertureless SNOM).

In this paper, we first describe the studied laser diode (Sect. 2). Next, we describe our experimental set-up (Sect. 3), and then, we show and discuss the influence of several experimental parameters leading to near-field optical images that we comment (Sect. 4). In Section 5, we conclude and evoke some perspectives.

* This paper was presented at the special CFMCP colloquium held at Strasbourg-Illkirch the July 1st-3rd, 1998.

^a e-mail: renaud.bachelot@univ-troyes.fr

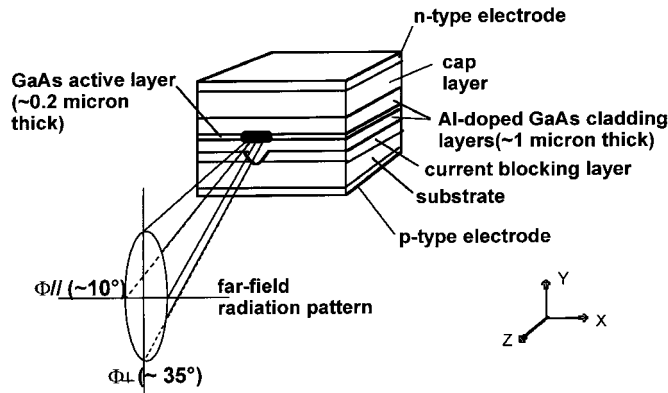


Fig. 1. Schematic diagram of the structure of the double hetero-junction laser diode studied in the near-field zone (see text for precise description). The Y axis is parallel to the growth direction. During near-field imaging, the axis of the probe tip is parallel to the Z axis and the scan is in the (X, Y) plane.

2 Description of the studied laser diode

Figure 1 represents schematically the studied sample which is a commercial laser diode (SHARP LT020MC, V-grooved Substrate Internal Stripe (VSIS) structure, $\lambda = 780$ nm, max. optical power = 3 mW) whose protection window has been removed. It is made of a double hetero-junction ($\text{Ga}_{1-x}\text{Al}_x\text{As}/\text{Ga}_{1-y}\text{Al}_y\text{As}/\text{Ga}_{1-x}\text{Al}_x\text{As}$, with $y = 0.15$ because $\lambda = 780$ nm [10]) constituting a potential well [10–12] whose emission area is represented in black in Figure 1. The centered active layer structure (VSIS structure) uses a much thicker p -type cladding layer to effectively move the emission point closer to the chip center by confining the injection current and the laser oscillation to a narrow strip. This special structure acts as an optical waveguide in both longitudinal (due to the VSIS structure) and transverse (due to the low refractive index of the cladding layers) directions, respectively called X et Y in Figure 1.

Because of its structure, this “index-guided” laser generates a single transverse mode whose far-field intensity pattern is pseudo-Gaussian, analogously to the TEM_{00} mode of many gas lasers, but elliptic in shape. The polarization state of the emitted light is elliptic with the electric vector mainly parallel to the junction plane (to the X axis). We worked with two values of the injection current: 20 mA and 45.6 mA. These values correspond to spontaneous emission and stimulated emission respectively, the threshold current being equal to 41 mA.

3 Experimental set-up

Our apertureless near-field optical microscope has been developed from a commercial SPM (Scanning Probe Microscope, model M5 from Park Scientific Instruments). The detailed description of this apertureless SNOM is given in reference [13].

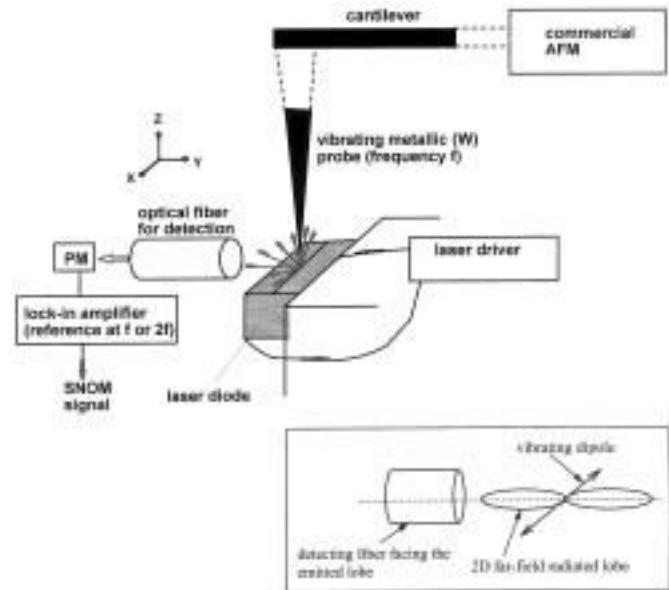


Fig. 2. Experimental SNOM configuration. The laser crystal is represented in gray, with emitting facet beneath the probe. The gray arrows represent the light emitted by the laser. PM: photomultiplier tube. Boxed: schematic diagram showing the far-field detection fiber that picks-up the propagating field emitted by the probe dipole. A “crossed analysis” of this field would be performed by placing the detection fiber parallel to the dipole axis (*i.e.* X axis).

The experimental configuration used here is shown in Figure 2. The sample is mounted on a XY step-motorized table, its front facet being perpendicular to the axis of the AFM tip. A commercial laser driver controls the pumping current. The tip vibrates perpendicularly to the sample and scans in near-field zone the emitting active region, while the tip-to-surface separation is controlled by an atomic force regulation in the intermittent-contact mode. Simultaneously, the optical scattered flux, from the tip end in local interaction with the sample, is far-field collected by a photomultiplier *via* an optical fiber (100 μm core/140 μm cladding, numerical aperture = 0.48, probe-to-fiber distance $\cong 100$ μm). A lock-in detection provides the SNOM signal. The experiments have been performed using homemade tungsten tips manufactured by electrochemical etching [13]. Figure 3 shows the geometry of such a probe (cantilever + tip). The tip size is controlled by Scanning Electronic Microscopy (SEM). Its terminal radius is typically 20 nm. The choice of this kind of probe-tip is not arbitrary. Its shape (both the tip end-to-cantilever distance and the tip sharpness) should attenuate the perturbations of the laser compared to most of the commercial probes. In particular, multiple reflection between the laser and the cantilever should be avoided.

The far-field detection by an optical fiber, hold by a commercial micro-pipette-holder [13], permits us to easily adjust both direction and angles of the detection. Indeed, the optical flux scattered by the probe in the far-field is not spatially isotropic. Hence, the interaction between

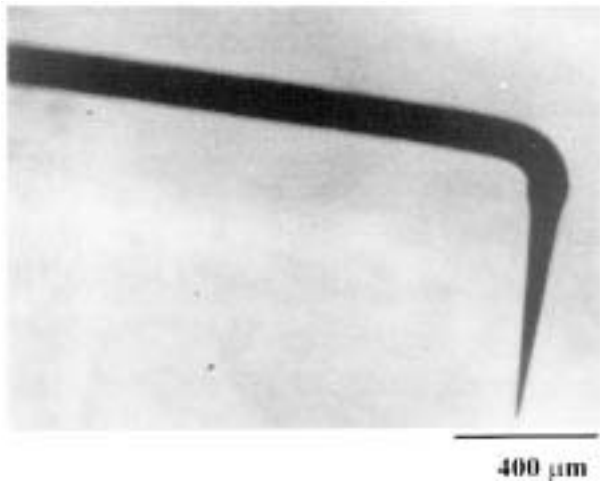


Fig. 3. 1.7 mm \times 1.2 mm size snapshot of a W metallic probe (cantilever and tip) used for the experiments (image obtained by optical microscopy).

the probe and the light emitted by the laser source gives rise to preferential scattering directions which depend, in particular, on the polarization state of the source [14]. In this way, this angular sensitive far-field detection can be useful for a polarization study of the sample [14]. The choice of the detection direction is of importance. Especially, we will see that a detection with a grazing angle leads to significant images. Indeed, it is obvious that not only the tip end is illuminated by the laser sample during the scan. Both the tip body and the cantilever are also illuminated (see Fig. 2). This gives rise to an unwanted background signal due to the forward scattered light which essentially radiates in directions other than the grazing one. Consequently, a grazing detection should significantly improve the signal to noise ratio (the term “signal” defines here the optical flux scattered only by the tip end). Assuming that the field emitted by the dipoles of the sample is mainly polarized parallel to the laser junction (to the X axis), a basic analysis, based on the fact that the extremity of the probe acts as an electric dipole [14], indicates that this dipole radiates in all the directions perpendicularly to the active layer, *i.e.* in the Y direction in Figure 2. Therefore, two complementary far-field detection directions at grazing angle appear interesting. The first direction can be chosen perpendicularly to the layers (fiber axis parallel to the Y direction, as represented in Fig. 2). In this case, the detection fiber faces the main lobe of the dipole radiation (see the insert in Fig. 2). The second detection direction (not represented in Fig. 2) would consist in a “crossed analysis” of the polarized field by placing the fiber parallel to the junction (fiber axis parallel to the X direction). Preliminary experiments, not presented in this paper, have indicated that the first configuration provides the best signal-to-noise ratio. For these reasons, our detection system presents this configuration.

The AFM measurements, simultaneously recorded with SNOM, have shown that thermal effects, due to the

tip illumination by the laser source, induce some modifications in the physical properties of the probe. Comparable effects have been reported elsewhere [3,15]. These effects, not presented in this paper, are the subject of present experiments in our laboratory. Nevertheless, an important damping of the AFM cantilever oscillation minimizes these effects.

4 Results and discussion

4.1 Improvement of the signal-to-noise ratio

In the intermittent-contact mode the tip oscillates at a frequency f near the resonance frequency (typically 4 kHz in the case of our W probes) of the cantilever. Its trajectory is perpendicular to the sample surface. Its vibration amplitude is adjusted at the desired value in the (10–200 nm) range and is kept constant during the scan. This AFM operating mode, associated with the lock-in detection providing the SNOM signal, should enhance the optical signal-to-noise ratio because only the electromagnetic field, in interaction with the vibrating probe (cantilever + tip), provides a modulated signal. However, only the optical flux coming from the extreme tip end interests us because only this flux is associated with high resolution. Grazing detection has been chosen for this reason.

The following section presents the study of two other parameters enhancing the contribution of this flux:

- reference frequency of the lock-in amplifier;
- amplitude of the probe vibration.

4.1.1 Influence of the lock-in detection frequency

Figure 4 shows an improvement of the optical near-field contrast when the lock-in detection frequency is switched from f (the probe vibration frequency) to $2f$. In this experiment, the laser works in spontaneous emission (injection current = 20 mA) and the vibration amplitude is 120 nm. Image 4b reveals a well spatially defined region whose surface does not exceed a few μm^2 . At contrary, in the image 4a some patterns are observed in regions other than the emitting surface of the laser diode. In particular, some trails appear in both parallel and perpendicular directions with regard to the orientation of the active zone. These trails correspond to a modulated optical signal coming from the entirety of the probe illuminated by the laser diode during the scan. Their spatial distribution can be explained by the experimental configuration used in this study (*cf.* Fig. 2). Indeed, they correspond to the light scattered by the tip body, towards the detection fiber, whereas the tip end is not yet in interaction with the small active region of the laser diode. They are thus unwanted far-field contributions which do not appear in Figure 4b. Consequently, a lock-in detection performed at $2f$ seems to be very sensitive to the scattered flux modulated only by the extremity of the probe. We interpret this behavior by the following reasoning. The vertical tip

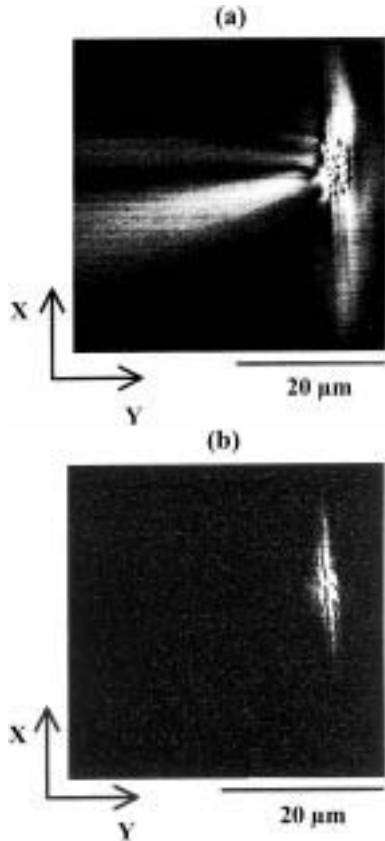


Fig. 4. SNOM images of the sample described in Figure 1 obtained by the experimental configuration of Figure 2. The probe scans the laser active zone in spontaneous emission with a vibration amplitude of 120 nm: (a) $40\ \mu\text{m} \times 40\ \mu\text{m}$ image provided by lock-in detection at the probe vibration frequency f , both the far-field and the near-field are present in the image, (b) $40\ \mu\text{m} \times 40\ \mu\text{m}$ image provided by lock-in detection at the frequency $2f$, the near-field part of the total modulated signal is predominant.

position is expressed by a sinusoidal function of the time. This is experimentally controlled when the microscope operates. When the tip is immersed in the optical field emitted by the laser, it scatters the optical far-field as well as the optical near-field during each period of its vibration. The near-field contains evanescent waves generated, by diffraction, by the high spatial frequencies of the sample surface [4,5,16]. Hence, in comparison to the amplitude of the tip vibration, the spatial extension (in the vertical direction) of the near-field is generally weak, and its gradient is very strong. This is, in particular, the case for our sample of very weak roughness and very sharp optical contrast. Therefore, the optical near-field, briefly viewed by the vibrating tip-end during each period of vibration, gives rise to very sharpened modifications in the sinusoidal time-function, generating a second harmonic component in the scattered flux. On the other hand, in images at f detection, the optical far-field contribution should be the principal component of the signal scattered by the tip during one period of oscillation. This qualitative argument is only an hypothesis which may explain the “near-field sen-

sitivity” of a $2f$ lock-in detection. Numerical simulations, demonstrating the importance of this non-linear effect, are in progress in our laboratory.

4.1.2 Influence of the probe vibration amplitude

To facilitate the extraction of the optical near-field component present in the scattered signal, the relative part coming from the sample near-field zone must be improved compared to the total modulated signal integrated by the lock-in amplifier. Hence, the vibration amplitude of the probe can play an important role in the filtering of the optical high frequencies. The purpose of this section is to show that the reduction of the vibration amplitude leads to an increased resolution. We have recorded images for several values of the probe vibration amplitude. Figures 5a and 5b, obtained for a vibration amplitude of 400 nm and 120 nm respectively, illustrate this resolution enhancement. In this experiment the laser worked in stimulated emission (injection current = 45.5 mA) and a f lock-in detection frequency was chosen. These experimental conditions were chosen because they permitted us to clearly show the following effect. Image 5b should be constituted principally from emission originating within the emitting area of the diode whereas the image obtained with 400 nm vibration (Fig. 5a) presents an important far-field contribution similar to that observed in Figure 4a.

Thus, the probe vibration amplitude is an important parameter to enhance the near-field contribution. Nevertheless, when the oscillation amplitude is lowered, the amplitude of the optical modulated signal may vary in the same way. This was particularly noticeable when the amplitude of vibration of the tip-end is lower than its terminal radius. The *danger* is then to pass under the sensibility of the far-field detection bench and thus to increase the cut-off detectable intensity in the images. This unwanted phenomenon could lead to an artificial resolution improvement, by threshold effect.

4.2 Near-field study of the laser diode in operation

The following sections report the near-field optical characterization of the laser diode in operation. Images have been performed with the laser in either spontaneous or stimulated emission. The experimental parameters take into account the conclusions of the previous sections: the oscillation amplitude was kept constant at 120 nm and a second harmonic lock-in detection was performed.

4.2.1 Laser diode working in stimulated emission

Figure 6a shows the intensity pattern obtained in stimulated emission (injection current = 45.5 mA). There are two hypothesis to interpret this image. The first assumption is to consider that the image coincides in shape and size with the geometrical active zone, *i.e.*, rectangular with the dimensions about $3.5\ \mu\text{m} \times 0.2\ \mu\text{m}$. In this case,

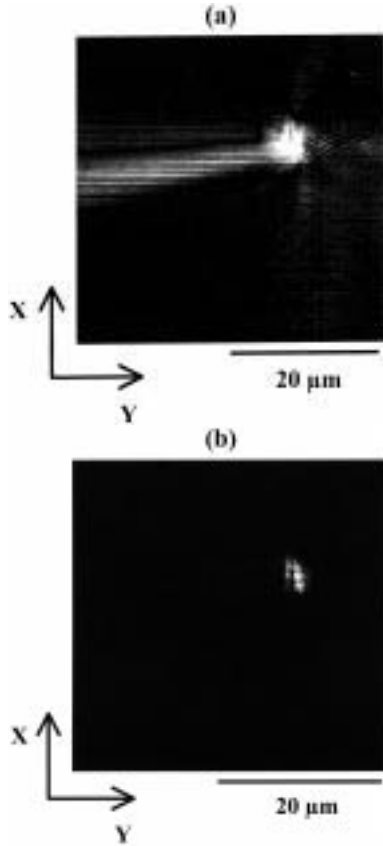


Fig. 5. Near-field images of the sample described in Figure 1 obtained by the SNOM configuration of Figure 2. The probe scans the active zone in stimulated emission. The optical images are provided by the lock-in amplifier at the frequency f . (a) $40\ \mu\text{m} \times 40\ \mu\text{m}$ image obtained with a probe vibration amplitude of $400\ \text{nm}$. The image contains a far-field contribution. (b) $40\ \mu\text{m} \times 40\ \mu\text{m}$ image obtained with a probe vibration amplitude of $120\ \text{nm}$. The near-field part of the signal scattered by the probe during a vibration period becomes predominant.

the rectangular aperture of the laser diode would act as the source. The second assumption is to consider that the real source is localized at farther distance from the laser diode output aperture and generates light which is guided in the active layer towards the output aperture. In this case, if we take into account that the wave-guide (in both lateral and longitudinal directions) is not “perfect” (the confinement factor Γ is not equal to 1) [10], then the image of the source would be oval with the dimensions of the laser mode [1]. Image 6a displays a unique intensity pattern resembling the single mode emission expected. The intensity distribution appears oval in shape (about $3.7 \times 1.5\ \mu\text{m}^2$) masking thus completely the geometrical active zone. Consequently, the sample surface would give an image of the optical mode of the laser diode. This is why we believe that the second assumption is more appropriate to interpret Figure 6a. Figure 7 shows that the obtained image of Figure 6a is in good agreement with both theoretical results and the specifications given by the manufacturer. Indeed, the cross-sections in Figure 7 reveal a width, measured at I_{max}/e^2 , of $3.7\ \mu\text{m} \times 1.5\ \mu\text{m}$ ($d_x \times d_y$) in the

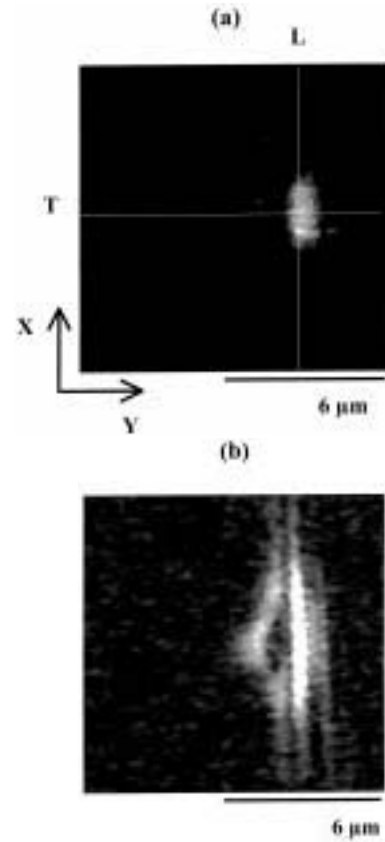


Fig. 6. Near-field images of the sample described in Figure 1 obtained by the SNOM configuration of Figure 2. The probe scans the active zone with a vibration amplitude of $120\ \text{nm}$. The optical images are provided by the lock-in amplifier at the frequency $2f$: (a) $12\ \mu\text{m} \times 12\ \mu\text{m}$ image obtained in stimulated emission (injection current = $45.5\ \text{mA}$), the emitted laser mode is imaged. (b) $12\ \mu\text{m} \times 12\ \mu\text{m}$ image obtained in spontaneous emission (injection current = $20\ \text{mA}$), showing a contrast linked to the refractive index contrast of the laser front facet. Cross-sections, of (a), along the transverse T and lateral L directions are shown in Figure 7.

X and Y directions respectively. Comparing Figure 7 and theoretical results of reference [10], the transverse confinement factor Γ_Y , related to the transversal expansion of the mode in the Y direction, is found equal to 0.4. This value of Γ_Y leads to the following composition of the cladding layers: $\text{Ga}_{0.7}\text{Al}_{0.3}\text{As}$. Typically, the Al molar fraction (x) of an $\text{Ga}_{1-x}\text{Al}_x\text{As}$ is inferior to 0.37 in order to make the stimulated emission process possible [10].

Usually, one evaluates the size of the emitted mode by numerical methods based on an inverse Fourier Transform of the far-field intensity distribution [12]. This leads to the knowledge of the size (d_x , d_y) of the emitted mode in near-field by measuring the angles ϕ_{\parallel} and ϕ_{\perp} , by the expressions: $d_x = \lambda/\phi_{\parallel}$, $d_y = \lambda/\phi_{\perp}$. In our case, using the experimental values of d_x and d_y , we calculated the far-field diffraction angles: $\phi_{\perp} = 30^\circ$ and $\phi_{\parallel} = 12^\circ$. These values are in good agreement with the values given by the manufacturer, *i.e.*, $35^\circ \times 11^\circ$.

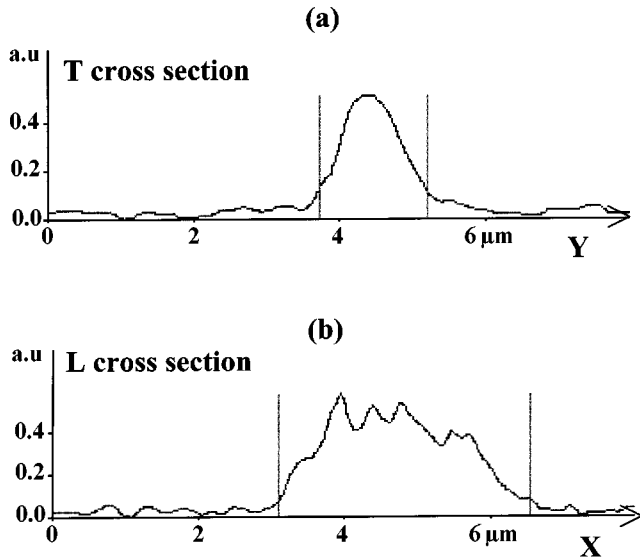


Fig. 7. Cross-sections from the emitted mode obtained in stimulated emission (Fig. 6a): (a) cross-section along the transverse T direction (Y direction in Fig. 1) showing a width, at I_{\max}/e^2 , of $1.5 \mu\text{m}$. (b) Cross-section along the lateral L direction (X direction in Fig. 1) showing a lateral width, at I_{\max}/e^2 , of $3.7 \mu\text{m}$. The vertical lines have been used for width measurements at $1/e^2$.

4.2.2 Laser diode working in spontaneous emission

Figure 6b shows the intensity pattern measured in spontaneous emission (injection current = 20 mA). Optical contrast can be observed not only in the expected emitting zone but also in adjacent regions. Several stripes are clearly visible. The respective shapes of these bands correspond to those of the layers which form the double heterojunction. Especially, we discern three parallel bands. One presents a “V” shape comparable to the VSIS structure of the p -type cladding layer (*cf.* Fig. 1). The two other stripes would thus correspond to the active layer and the n -type cladding layer. Therefore, in the case of spontaneous emission, a sample surface zone larger than the expected emitting one seems to be illuminated by the source. We interpret this behavior by the fact that the spontaneous process gives rise to photons emitted into a large angle cone. These photons do not satisfy the conditions of optical guiding in the active layer. A photon leakage occurs then in the surrounding layers which are consequently also illuminated. Thus, in this case our SNOM experiment seems able to describe a contrast linked to the refractive index contrast of the sample surface.

In summary, under the threshold current the SNOM images may give information about the physical structure (index contrast) of the laser diode front facet, whereas in stimulated emission they seem to be much more sensitive to the emitted optical mode. Buratto *et al.* came to the same conclusion using an aperture SNOM [1].

The near-field origin of the images presented in Section 4.2 has been confirmed by varying the average distance between the probe and the sample without vary-

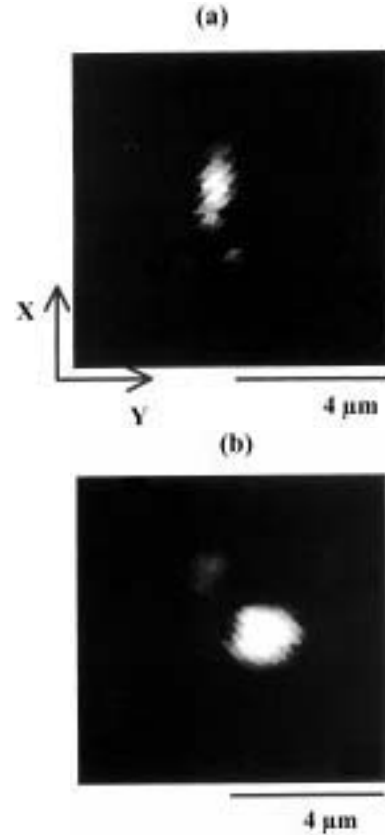


Fig. 8. Near-field images of the sample described in Figure 1 obtained by the SNOM configuration of Figure 2. The probe scans the active zone in stimulated emission with a vibration amplitude of 120 nm. (a) $8 \mu\text{m} \times 8 \mu\text{m}$ image obtained while the probe is in near-field interaction with the sample, near-field information are achieved. (b) $8 \mu\text{m} \times 8 \mu\text{m}$ image obtained while the probe-to-sample average distance was $3 \mu\text{m}$. An intermediate circular far-field diffraction pattern is observed.

ing the probe oscillation amplitude. Images of Figure 8 have been obtained with a probe oscillation amplitude of 120 nm and a pumping current of 45.5 mA. In images 8a and 8b, the average probe-to-sample gap was 120 nm (feedback loop in action) and $3 \mu\text{m}$ respectively. In the case of Figure 8a, the tip comes alternatively in interaction with the near-field, whereas in the Figure 8b the tip scatters only the far-field. In Figure 8a the intensity distribution appears oval and reflects approximately the shape of the emitted mode. A second pattern can be observed in Figure 8a. Its intensity is weaker than that of the oval pattern. Presently, we are ignorant of the origin of this second pattern. It can correspond to either an electroluminescence due to a local carrier leakage, as was observed by Buratto *et al.* [1], or a second scattering center of the probe-tip due to the specific shape of the tip end used for this image. When the probe is moved away from the sample surface (Fig. 8b) the intensity distribution (of the brightest pattern) consists roughly of a circular spot of diameter $3.6 \mu\text{m}$ at $1/e^2$. This shape is in agreement with the far-field diffraction (Fraunhofer diffraction)

of the near-field pattern (the elliptic emitting zone of the laser). Indeed, this Fraunhofer diffraction pattern is an ellipse oriented at 90° with regard to the near-field pattern (see Fig. 1). An intermediate diffraction pattern is circular, comparable in shape to that observed in Figure 8b. This phenomenon, also observed by Ben-Ami *et al.* [2], confirms that both Figures 8a and 6a are dominated by information coming from the optical near-field of the laser diode.

5 Conclusions and perspectives

In conclusion, we have shown that this apertureless SNOM configuration is able to study active samples in the near-field. In particular, the study of a GaAlAs double heterojunction has demonstrated that the apertureless SNOM gives complementary information in stimulated and spontaneous emission. In stimulated emission, images of the laser mode are displayed, whereas in spontaneous emission information specific to the spontaneous phenomenon are obtained permitting the qualitative description of the laser front facet structure in terms of refractive index contrast. Experimental parameters making the laser diode study possible have been chosen with care taking account of the optical properties own on this sample. The optimal probe vibration amplitude, the second harmonic lock-in detection, as well as the suitable far-field collection direction have been determined to permit the near-field signal extraction.

The study of both the influence of the detection fiber position and the thermally induced mechanical effects are in progress. Furthermore, we will extend this work to several types of laser diodes as well as to other opto-electronic

components (optical guides and integrated optical components).

The authors are grateful to R. Deturche for sample preparation, and to P.M. Adam, O. Bergossi, and S. Hudley for their review of this paper and helpful discussion.

References

1. S.K. Buratto *et al.*, *J. Appl. Phys.* **76**, 7720 (1994).
2. U. Ben-Ami *et al.*, *Appl. Phys. Lett.* **68**, 2337 (1996).
3. Ch. Lienau, A. Richter, T. Elsaesser, *Appl. Phys. Lett.* **69**, 325 (1996).
4. J.P. Fillard, *Near-Field Optics and Nanoscopy* (World Scientific, Singapore, 1996).
5. M.A. Paesler, P.J. Moyer, *Near-field Optics* (John Wiley & Sons Inc., New York, 1996).
6. Y. Inouye, S. Kawata, *Opt. Lett.* **19**, 159 (1994).
7. R. Bachelot, P. Gleyzes, A.C. Boccarda, *Opt. Lett.* **20**, 1924 (1995).
8. F. Zenhausern, Y. Martin, H.K. Wickramasinghe, *Science* **269**, 1083 (1995).
9. A. Lahrech *et al.*, *Opt. Lett.* **21**, 1315 (1996).
10. H.C. Casey, M.B. Panish, *Heterostructure lasers* (Academic Press, 1978).
11. S.L. Chuang, *Physics of optoelectronic devices* (John Wiley & Sons Inc., New York, 1995).
12. E. Rosencher, B. Vinter, *Optoélectronique* (Masson, Paris, 1998).
13. G. Wurtz, R. Bachelot, P. Royer, *Rev. Sci. Instr.* **69**, 1735 (1998).
14. A. Madrazo *et al.*, *J. Opt. Soc. Am. A* **15**, 109 (1998).
15. S. Grafström *et al.*, *J. Appl. Phys.* **83**, 3453 (1997).
16. O. Bryngdahl, in *Progress in Optics XI*, edited by E. Wolf (North-Holland, 1973).